Calculation of the Thermoelectric Properties of *n*- and *p*-Type Lead Telluride Using a Three-Band Model of the Electron Energy Spectrum

A.V. DMITRIEV[1,2] and E.S. TKACHEVA[1]

1.—The Faculty of Physics, Moscow State University, Moscow 119991, Russia. 2.—e-mail: dmitriev@lt.phys.msu.su

In this paper, we study theoretically the thermoelectric properties of *n*- and *p*-type PbTe in the wide temperature interval of 300–900 K. A three-band model of the PbTe electron energy spectrum is used in these calculations. The full set of the relevant kinetic characteristics is calculated including the electrical and thermal conductivities, the Seebeck coefficient, and the thermoelectric figure-of-merit. The calculated thermoelectric quantities are in good agreement with the available experimental data.

INTRODUCTION

Energy production and conversion are among the most important activities of human civilization and, indeed, the cornerstone of its existence. The primary concern and the subject of continual research and development effort is, of course, to effectively produce electric energy, the most universal and convenient one for practical applications. As the lack of fossil fuel is being increasingly recognized and huge greenhouse gas emissions from organic fuel power plants are producing global climate changes, the efficient conversion of heat energy to electric energy is becoming a problem of vital importance.

In this connection, much attention has been focused on solid-state thermoelectric converters. They offer a number of advantages over traditional electric generators, including design simplicity, absence of moving parts, low-noise performance, high reliability, and miniaturization without loss in efficiency. As bidirectional energy converters, they are also used in eco-friendly cooling systems.

Currently, however, thermoelectric devices are lower in conversion efficiency compared to the traditional designs of electric generators or refrigerators and have therefore not found wide application in industry. But there exist application areas where the advantages of these devices prevail over their disadvantages. Examples include power sources for spacecrafts, wrist watches, portable household refrigerators, electronic, medical, and research equipment (in particular, that for cooling infrared detectors and optoelectronic devices), and even seat conditioning devices in luxury cars.

As the application area of thermoelectric devices is very wide, it is not surprising that different materials have advantages in different conditions. For high-temperature applications, PbTe and its alloys are among the best-known materials with the thermoelectric figure-of-merit

$$ZT = \frac{\sigma S^2 T}{\kappa} \tag{1}$$

approaching 0.7 at T = 700–800 K.[1–3] In Eq. 1, σ is the electrical conductivity, S the Seebeck coefficient, and κ the heat conductivity of the material.

PbTe is a narrow-gap semiconductor (Fig. 1), and many impurities are known to form deep levels or impurity bands in it, either in the fundamental gap or on the background of the conductivity or valence band of the crystal.[5–9] A rapid variation of the density of states in the vicinity of a narrow impurity band can lead to a significant increase of the

Calculation of the Thermoelectric Properties of *n*- and *p*-Type Lead Telluride Using
a Three-Band Model of the Electron Energy Spectrum

1281

Seebeck coefficient and hence of the figure-of-merit according to the well-known Mott formula[10] applicable to degenerate semiconductors:

$$S = \frac{\pi^2 T}{3e} \frac{\partial \ln \sigma}{\partial E}\bigg|_{E=E_F} = \frac{\pi^2 T}{3e} \frac{\partial \ln(v^2 g\tau)}{\partial E}\bigg|_{E=E_F}. \quad (2)$$

Here, v is the carrier velocity, τ the carrier relaxation time, and g the density of states. And, indeed, a significant increase of ZT up to 1.5 at 700 K was observed in *p*-type PbTe co-doped with Tl and Na, which was attributed to the influence of a Tl impurity band.[11]

However, it has been shown that a similar increase of the figure-of-merit could be obtained using only intrinsic features of the PbTe energy spectrum. In reality, the density of states also increases sharply in a vicinity of an extremum of a crystal band, i.e. of the Van Hove singularity. The heavier the band, the more rapid the increase, so, in PbTe, the heavy hole Σ-band is the most promising (Fig. 1). This idea was realized in Refs. 12 and 13, and an increase of ZT up to 1.3 at 700 K has been observed in *p*-type PbTe heavily co-doped with K and Na, so that the hole's Fermi level is situated close to the Σ-band edge[13]. Similar results were also obtained in Ref. 14.

In this paper, we develop a theoretical description of the latter situation. As the figure-of-merit in PbTe is at maximum at the high temperatures around 700 K, the correct description of the electron kinetics requires that carrier transport over all three crystal bands situated in the vicinity of the Fermi level be taken into account: the electron and light hole bands with the extrema in L-points of the Brillouin zone and the heavy hole band with the maxima in Σ-points. Three-band carrier kinetics is rather complicated but allows a unified description of the thermoelectric phenomena in the wide temperature and doping interval of 300–900 K at donor and acceptor concentrations up to $10^{19}/\text{cm}^3$.

MODEL DESCRIPTION

PbTe is a cubic crystal, and its conductivity is isotropic. So we use in our calculations an isotropic model of its band spectrum.* An important feature of the electron and light hole dispersion laws is their strong non-parabolicity, and we take it into account using the Lax spectrum model in the L-point extrema. In the Luttindger–Cohn representation the Hamiltonian of this model can be written in the formally relativistic form

$$\hat{H}(\mathbf{k}) = \frac{E_g}{2}\hat{\beta} + V\hat{\alpha}\mathbf{k}, \quad (3)$$

that looks similar to the Dirac Hamiltonian in which $E_g/2$ stays instead of mc^2 and a limiting electron velocity $V \sim 10^8$ cm/s takes place of the light velocity, $\hat{\alpha}_i$ and $\hat{\beta}$ are the Dirac matrices, $\mathbf{k}$ is the momentum calculated from the L-point.[16]

This Hamiltonian leads to the non-parabolic energy dispersion laws of the electrons and light holes:

$$E_{\mp}(k) = \pm\sqrt{\frac{E_g^2}{4} + V^2 k^2}, \quad (4)$$

where the upper signs correspond to the conductivity band and the lower to the valence one. The energy is calculated from the middle of the direct gap in the L-points.

The electron and hole states that correspond to the Hamiltonian (3) are doubly degenerate according to Kramers theorem. These states are equivalent in kinetics so we will not distinguish between them and will describe them by a density matrix that contains both states in equal portions. In the Luttinger–Cohn basis, the density matrices have the form

$$\hat{\rho}_{\mp}(\mathbf{k}) = \frac{\hat{H}(\mathbf{k}) - E_{\pm}\hat{I}}{\text{Sp}\left[\hat{H}(\mathbf{k}) - E_{\pm}\hat{I}\right]} = \frac{E_{\mp}(\mathbf{k})\hat{I} + \hat{H}(\mathbf{k})}{4E_{\mp}(\mathbf{k})}, \quad (5)$$

$\hat{I}$ being the unit matrix.** Then, the only characteristic of an electron state in a band, either the conductivity or the valence one, becomes its momentum $\mathbf{k}$.

Other important functions connected with the energy spectrum are the density of states g, the carrier velocity v, the momentum k expressed through the energy and the effective mass at the
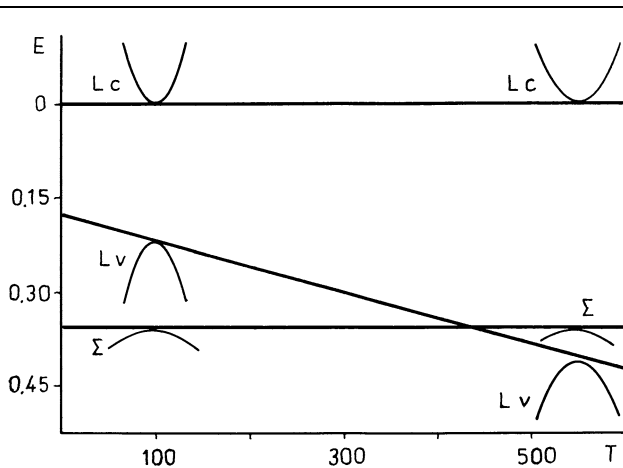

Fig. 1. Diagram of PbTe electron energy spectrum variation with temperature (drawn according to the data in Ref. 4). *Lc* conductivity band minima in L-points of the Brillouin zone, *Lv* valence band maxima in L-points, Σ are the heavy hole extrema in Σ-points. Energy is in eV, temperature in K.

---

*An attempt to calculate the Seebeck coefficient of PbTe using an anysotropic model of its spectrum was recently performed in Refs. 12 and 15.

**The expression (5) is evident in the basis of the eigenfunctions of the Hamiltonian where the latter is diagonal.

band edges m^*. All four do not differ for electrons and holes:

$$g(E) = \frac{8\pi}{(2\pi\hbar)^3} \frac{E_g^2}{V^3} \epsilon \sqrt{\epsilon^2 - 1/4}, \qquad (6)$$

$$v(E) = V \frac{\sqrt{\epsilon^2 - 1/4}}{\epsilon}, \qquad (7)$$

$$k(E) = \frac{E_g}{V} \sqrt{\epsilon^2 - 1/4}, \qquad (8)$$

$$m^* = \frac{E_g}{2V^2}, \qquad (9)$$

where $\epsilon = E/E_g$. The Kramers degeneracy has been taken into account in Eq. 6. The light carrier effective mass at the Fermi level

$$m^*(E_F) = \left(\frac{\partial^2 E}{\partial k^2}\right)^{-1}\Bigg|_{E=E_F}$$

lies in the interval $(0.02 \div 0.15)m_0$, depending on the doping concentration.

CARRIER CONCENTRATION

Using the expression (6) for the density of states and introducing dimensionless variables $x = E/T = (E_g/T)\epsilon$ and $\eta = \mu/T$, μ being the chemical potential, we come to the following expression for the carrier density in either the conductivity or the valence band:

$$n = \frac{E_g T^2}{\pi^2 \hbar^3 V^3} \int_{\frac{E_g}{2T}}^{\infty} \frac{x\,dx}{1 + \exp(x-\eta)} \sqrt{\left(\frac{Tx}{E_g}\right)^2 - \frac{1}{4}}. \qquad (10)$$

After the shifting of the energy origin to the band edge for computational convenience, one obtains

$$n = \frac{E_g^2 T}{\pi^2 \hbar^3 V^3} \int_0^{\infty} \frac{dx}{1 + \exp(x-\eta)} \left(\frac{Tx}{E_g} + \frac{1}{2}\right) \sqrt{\left(\frac{Tx}{E_g}\right)^2 + \frac{Tx}{E_g}}, \qquad (11)$$

and similarly for the light holes but with the other η sign. The expression for the heavy holes is also similar but with a different E_g value, see Eq. 39.

In the thermodynamical equilibrium, the electrons in all bands are characterized by one chemical potential that can be found from the electroneutrality condition:

$$n - p - p_\Sigma - N_d + N_a = 0,$$

where n, p and p_Σ are the concentrations of electrons and holes in L-bands and of holes in Σ-band, respectively; N_d and N_a are the donor and acceptor concentrations.

This equation was solved numerically with respect to the chemical potential μ for every temerature and doping level combination, and the μ value found this way was used in subsequent calculations of the kinetic coefficients.

RELAXATION TIMES

At elevated temperatures, even optical phonon scattering can be considered quasi-elastic so the relaxation time approximation can be used for the calculation of the kinetic quantities with the transport relaxation time defined as

$$\frac{1}{\tau} = \sum_{\mathbf{k}'} W(\mathbf{k} \to \mathbf{k}')(1 - \cos\theta), \qquad (12)$$

where $W(\mathbf{k} \to \mathbf{k}')$ is the carrier interband transition probability from the state $\mathbf{k}$ to $\mathbf{k}'$, and θ is the scattering angle, that is, the angle between $\mathbf{k}$ and $\mathbf{k}'$. This expression is valid for any band.

Impurity Scattering

As we use the mixed electron band states, the probability W in (12) is the actual transition probability w averaged over the initial and final band branch indices:

$$\begin{aligned}
W_I(\mathbf{k} \to \mathbf{k}') &= \frac{1}{4} \sum_{\substack{i=1,2 \\ j=1,2}} w_I(\mathbf{k},i \to \mathbf{k}',j) \\
&= \frac{2\pi}{\hbar} N_I \frac{1}{4} \sum_{\substack{i=1,2 \\ j=1,2}} \hat{V}_{\mathbf{k},i;\mathbf{k}',j}^2 \delta(E(k) - E(k')) \\
&= \frac{2\pi}{\hbar} N_I V(\mathbf{k} - \mathbf{k}')^2 \delta(E(k) - E(k')) \\
&\quad \times \frac{1}{4} \sum_{\substack{i=1,2 \\ j=1,2}} \langle \mathbf{k},i | \mathbf{k}',j \rangle^2 \\
&= \frac{2\pi}{\hbar} N_I V(\mathbf{k} - \mathbf{k}')^2 \overline{I(\mathbf{k},\mathbf{k}')^2} \delta(E(k) - E(k')),
\end{aligned} \qquad (13)$$

where N_I is the impurity concentration, $\hat{V}_{\mathbf{k},i;\mathbf{k}',j}$ is the matrix element of the Coulomb impurity potential corresponding to the transition, and $V(\mathbf{k} - \mathbf{k}')$ is the Fourier transform of the Coulomb potential:

$$V(\mathbf{k}) = \frac{4\pi e^2}{\varepsilon_0} \left(\frac{\hbar}{k}\right)^2, \qquad (14)$$

ε_0 is the static dielectric constant, $|\mathbf{k},i\rangle \equiv U_{\mathbf{k},i}(\mathbf{r})$ is the Bloch amplitude of the carrier wave function in the ith branch of the band.

The averaged overlap integral

Calculation of the Thermoelectric Properties of *n*- and *p*-Type Lead Telluride Using
a Three-Band Model of the Electron Energy Spectrum

1283

$$\overline{I(\mathbf{k},\mathbf{k}')^2} = \frac{1}{4}\sum_{\substack{i=1,2\\j=1,2}} \langle \mathbf{k},i|\mathbf{k}',j\rangle^2$$

$$= \frac{1}{4}\sum_{\substack{i=1,2\\j=1,2}} \int d^3\mathbf{r}\, U^*_{\mathbf{k},i}(\mathbf{r}) U_{\mathbf{k}',j}(\mathbf{r}) \qquad (15)$$

$$= \mathrm{Sp}\big[\rho(\mathbf{k})\rho(\mathbf{k}')\big] = \frac{\epsilon^2(\mathbf{k}) + \mathbf{k}\mathbf{k}' + 1/4}{4\epsilon^2(\mathbf{k})}$$

describes an additional angle dependence of the scattering probability caused by the Bloch amplitudes of the wave functions, and ρ being the density matrices of the corresponding band (see Eq. 5). Due to the low-angle character of the Coulomb scattering

$$|\mathbf{k}-\mathbf{k}'| \ll k,k', \quad \overline{I^2} \approx 1.$$

Substituting (13) into (12) and taking into account the expressions (4), (7) and (8), one obtains

$$\frac{1}{\tau_I} = \frac{4\pi L N_I e^4}{\varepsilon_0^2 v k^2} = \frac{4\pi L N_I e^4 V\epsilon}{\varepsilon_0^2 E_g^2 (\epsilon^2 - 1/4)^{3/2}}, \qquad (16)$$

where L is the Coulomb logarithm.

As the Lax spectrum is mirror-simmetric, this expression is evidently valid for either the electron and the light hole band.

Introducing again the dimensionless variable $x = E/T$ instead of $\epsilon = E/E_g$, one has

$$\frac{1}{\tau_I} = \frac{4\pi L N_I e^4 VT}{\varepsilon_0^2 E_g^3} x\left[\left(\frac{Tx}{E_g}\right)^2 - \frac{1}{4}\right]^{-3/2}, \qquad (17)$$

and after the shift of the energy origin to the band edge, one comes to the final expression

$$\frac{1}{\tau_I} = \frac{4\pi L N_I e^4 V}{\varepsilon_0^2 E_g^2}\left(\frac{Tx}{E_g} + \frac{1}{2}\right)\left[\left(\frac{Tx}{E_g}\right)^2 + \frac{Tx}{E_g}\right]^{-3/2}. \qquad (18)$$

Acoustic Phonon Scattering

Let us consider the electron-deformation acoustic phonon interaction. The interaction Hamiltonian is taken in the simple form

$$\hat{H}_{e-DA} = C_1 \ \mathrm{div}\ \mathbf{U}(\mathbf{r}) \cdot \hat{I}, \qquad (19)$$

where C_1 is the deformation potential, $\mathbf{U}(\mathbf{r})$ is the lattice displacement vector in the continuous medium approximation, and $\hat{I}$ is the unit operator with respect to the electron states in the Luttindger–Cohn basis.

Within elastic scattering approximation and assuming equipartition of phonons, the Hamiltonian (5) leads to the following transition probability:

$$w_{DA}(\mathbf{k},i \to \mathbf{k}',j) = \frac{2\pi T_0 C_1^2}{\hbar \Omega \varrho_m s^2}|\langle \mathbf{k},i|\mathbf{k}',j\rangle|^2 \delta(E(k) - E(k')), \qquad (20)$$

where T_0 is the lattice temperature, ρ_m and Ω is the mass density and volume of the crystal, and s is the sound velocity.

Averaging the probability over the band branch indices, i and j, which reduces to the substitution of $\mathrm{Sp}[\hat{\rho}_\mp(\mathbf{k})\hat{\rho}_\mp(\mathbf{k}')]$ in place of $|\langle \mathbf{k},i|\mathbf{k}',j\rangle|^2$ in the Eq. 20, the upper signs being valid for the conductivity band and the lower ones for the valence band, one comes to the expression for the average transition probability:

$$W_{DA}(\mathbf{k} \to \mathbf{k}') = \frac{\pi T_0 C_1^2}{2\hbar \varrho_m \Omega s^2}\frac{\epsilon^2(\mathbf{k}) + \mathbf{k}\mathbf{k}' + 1/4}{\epsilon^2(\mathbf{k})}$$
$$\times \delta(E(k) - E(k')). \qquad (21)$$

The corresponding relaxation time (12) can now be easily calculated:

$$\frac{1}{\tau_{DA}} = \frac{C_1^2 T_0 E_g^2}{6\pi\hbar^4 \varrho_m s^2 V^3}\frac{(2\epsilon^2 + 1)\sqrt{\epsilon^2 - 1/4}}{\epsilon}. \qquad (22)$$

In terms of $x = E/T$ it becomes

$$\frac{1}{\tau_{DA}} = \frac{C_1^2 E_g^3}{6\pi\hbar^4 \varrho_m s^2 V^3 x}\sqrt{\left(\frac{Tx}{E_g}\right)^2 - \frac{1}{4}}\left[2\left(\frac{Tx}{E_g}\right)^2 + 1\right], \qquad (23)$$

and calculating the energy from the band edge, one comes to the final expression:

$$\frac{1}{\tau_{DA}} = \frac{C_1^2 E_g^2 T}{6\pi\hbar^4 \varrho_m s^2 V^3}\sqrt{\left(\frac{Tx}{E_g}\right)^2 + \frac{Tx}{E_g}}$$
$$\times \left[2\left(\frac{Tx}{E_g} + \frac{1}{2}\right)^2 + 1\right]\left(\frac{Tx}{E_g} + \frac{1}{2}\right)^{-1}. \qquad (24)$$

This formula is applicable to either the conductivity or the valence band.

Polar Optical Phonon Scattering

At higher temperatures, this is the most effective carrier scattering mechanism in a polar crystal such as lead telluride. The corresponding averaged electron transition probability due to absorption and emission of an PO-phonon with the frequency ω and momentum q in the elastic approximation equals

$$W(\mathbf{k} \to \mathbf{k}') = W(\mathbf{k},\mathbf{k} \pm \mathbf{q})$$
$$= 4\pi^2 e^2\hbar^2\omega\left(\frac{1}{\varepsilon_\infty} - \frac{1}{\varepsilon_0}\right)\frac{\overline{I(\mathbf{k},\mathbf{k}')^2}}{q^2}$$
$$\times (2f_0 + 1)\delta(E(k) - E(k')), \qquad (25)$$

where

$$f_0 = \frac{1}{\exp(\hbar\omega/T) - 1}$$

is the PO-phonon distribution function, ε_0 is the static dielectric contant, and ε_∞ the high-frequency one.

The formula (25) differs from the standard expression[17] as it contains the overlap integral for the Lax spectrum.[†]

In the elastic approximation, $k'^2 = k^2$ and

$$q^2 = (\mathbf{k}' - \mathbf{k})^2 = \mathbf{k}'^2 - 2\mathbf{k}\mathbf{k}' + \mathbf{k}^2 = 2k^2(1 - \cos\theta),$$

θ is the scattering angle. Substituting this into the probability (25) and farther into the relaxation time (12), one comes to the expression

$$\frac{1}{\tau_{PO}} = \int \frac{2 d^3\mathbf{k}'}{(2\pi\hbar)^3} \frac{2\pi^2 e^2 \omega \hbar^2 V^2}{E_g^2}$$
$$\times \left(\frac{1}{\varepsilon_\infty} - \frac{1}{\varepsilon_0}\right) \frac{\epsilon^2 + k^2\cos\theta + 1/4}{4\epsilon^2 k^2}$$
$$\times (2f_0 + 1)\delta(E(k') - E(k)). \qquad (26)$$

The term proportional to $\cos\theta$ disappears after the angle integration, and the integral of the δ-function gives the density of states

$$g(E) = \frac{8\pi}{(2\pi\hbar)^3 V^2} E_g \epsilon k$$

(see Eqs. 6 and 8), so one gets

$$\frac{1}{\tau_{PO}} = \frac{2e^2\omega}{\hbar V}\left(\frac{1}{\varepsilon_\infty} - \frac{1}{\varepsilon_0}\right)(2f_0 + 1)\frac{\epsilon^2 + 1/4}{4\epsilon k}. \qquad (27)$$

Introducing, as above, the dimensionless variable

$$x = \frac{1}{T}\left(E - \frac{E_g}{2}\right) = \frac{E_g}{T}\left(\epsilon - \frac{1}{2}\right),$$

one transforms the PO-phonon realxation time to the final form

$$\frac{1}{\tau_{PO}} = \frac{e^2\omega}{2\hbar V}\left(\frac{1}{\varepsilon_\infty} - \frac{1}{\varepsilon_0}\right)(2f_0 + 1)\left[\left(\frac{xT}{E_g}\right)^2 + \frac{xT}{E_g} + \frac{1}{2}\right]$$
$$\times \left[\sqrt{\frac{xT}{E_g}\left(\frac{xT}{E_g} + 1\right)}\left(\frac{xT}{E_g} + \frac{1}{2}\right)\right]^{-1}. \qquad (28)$$

Now, all carrier relaxation times have been calculated and the resulting full transport relaxation

[†]The overlap integral is band spectrum-specific. For example, a similar expression for PO-scattering transition probability for electrons in the Kane spectrum[18] also contains an overlap integral, but one different from Eq. 15.

time, $\tau(E)$, can be expressed through them according to Mathiessen's rule.

KINETIC COEFFICIENTS

The thermoelectric coefficients are calculated as a solution of the Boltzmann transport equation in the τ-approximation (see, e.g., Ref. 19). The thermoelectric coefficients can be expressed as functions of the kernel

$$\Sigma(E) = \sum_{\mathbf{k}} v_x^2(\mathbf{k})\tau(\mathbf{k})\delta(E - E(\mathbf{k})) = g(E)v_x^2(E)\tau(E), \qquad (29)$$

where $g(E)$ is the density of states, $v_x(\mathbf{k})$ is the group velocity of carriers with the momentum $\mathbf{k}$ in the direction x of the applied field, and τ is the transport relaxation time.

The electrical conductivity σ, Seebeck coefficient S and electron heat conductivity κ_0 found in this way are given for each band by the following formulae:

$$\sigma = e^2 \int_{-\infty}^{\infty} dE\left(-\frac{\partial f}{\partial E}\right)\Sigma(E), \qquad (30)$$

$$S = \frac{e}{T\sigma} \int_{-\infty}^{\infty} dE\left(-\frac{\partial f}{\partial E}\right)\Sigma(E)(E - \mu), \qquad (31)$$

$$\kappa_0 = \frac{1}{T} \int_{-\infty}^{\infty} dE\left(-\frac{\partial f}{\partial E}\right)\Sigma(E)(E - \mu)^2, \qquad (32)$$

where μ is the chemical potential, and $f(E)$ is the carrier Fermi distribution function, so that

$$\frac{\partial f}{\partial E} = -\frac{1}{T}\frac{\exp\left[(E - \mu)/T\right]}{\{\exp\left[(E - \mu)/T\right] + 1\}^2}. \qquad (33)$$

The heat conductivity κ_0 corresponds to a zero chemical potential gradient in the sample. It is connected with the usual electron heat conductivity $\kappa_{carrier}$ that corresponds to a zero electrical current and enters the figure-of-merit, by the formula

$$\kappa_{carrier} = \kappa_0 - T\sigma S^2. \qquad (34)$$

As there are three bands in the spectrum and, correspondingly, three carrier groups, namely, electrons in L-extrema (e), light holes in L-extrema (lh), and heavy holes in Σ-extrema (hh), the resulting formulae for the kinetic coefficients become rather complicated:[20–22]

$$\sigma = \sigma_e + \sigma_{lh} + \sigma_{hh}, \qquad (35)$$

Calculation of the Thermoelectric Properties of *n*- and *p*-Type Lead Telluride Using a Three-Band Model of the Electron Energy Spectrum

1285

$$S = \frac{S_e \sigma_e + S_{lh} \sigma_{lh} + S_{hh} \sigma_{hh}}{\sigma_e + \sigma_{lh} + \sigma_{hh}}, \tag{36}$$

$$\kappa = \kappa_{lattice} + \kappa_e + \kappa_{lh} + \kappa_{hh} + T\frac{\sigma_e \sigma_{lh}}{\sigma_e + \sigma_{lh}}(S_e + S_{lh})^2$$
$$+ T\frac{\sigma_e \sigma_{hh}}{\sigma_e + \sigma_{hh}}(S_e + S_{hh})^2 + T\frac{\sigma_{lh} \sigma_{hh}}{\sigma_{lh} + \sigma_{hh}}(S_{lh} - S_{hh})^2, \tag{37}$$

where $\kappa_{lattice}$ is the lattice thermal conductivity. We used the following approximate expression for it:[23]

$$\kappa_{lattice} T = 4.75 \text{ W/cm}. \tag{38}$$

The calculations according to the formulae above were performed numerically using the following values of the material parameters:[24–28]

$$E_{g,L} \text{ [eV]} = 0.19 + 4 \cdot 10^{-4}\, T \text{ [K]}, \quad E_{g,\Sigma} \text{ [eV]} = 0.36,$$
$$V = 1 \cdot 10^8 \text{ cm/s}, \quad s = 5 \cdot 10^5 \text{ cm/s},$$
$$C_1 = 10 \text{ eV}, \quad \hbar\omega = 14 \text{ meV},$$
$$\varepsilon_0 = 400, \quad \varepsilon_\infty = 33,$$
$$\varrho_m = 8.5 \text{ g/cm}^3, \quad L = 5. \tag{39}$$

The effective mass of heavy holes in Σ-extrema was taken as equal to the free electron mass, m_0. The parameters of the heavy holes and even the positions of their extrema in the Brillouin zone are not known precisely,[4,12,24] so we used the data presented in Ref. 24.

RESULTS

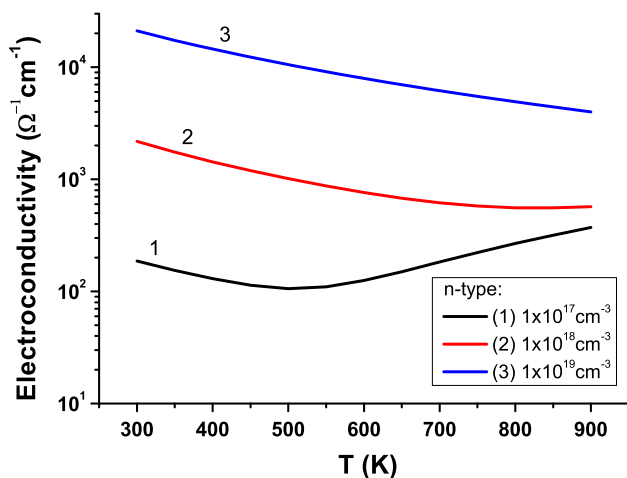The results of our calculations of the kinetic quantities of lead telluride are presented in Figs. 2–9.

Figures 2 and 3 show a normal semiconductor temperature dependence of the conductivity at low carrier density, with similar electron and hole mobilities (note the different conductivity scales in the two figures). Holes here are in L-extrema and their effective mass is equal to that of electrons. The conductivity increase with the temperature is due to thermal activation of additional carriers. At high acceptor concentration, the Fermi level moves to the heavy hole Σ-band so the average hole mobility decreases. In both electron and hole heavily doped materials, the conductivity diminishes as the temperature is raised because of predominate phonon scattering.

The temperature dependence of the Seebeck coefficient S is shown in Figs. 4 and 5. One can see that, as one would expect, the maximum of the absolute value of S that corresponds to the Fermi level position close to a band edge moves to higher temperatures for higher doping levels in both *n*- and *p*-type material. At a temperature around 800 K, the donor doping level of around $1 \cdot 10^{18}/\text{cm}^3$ or acceptor doping level close to $1 \cdot 10^{19}/\text{cm}^3$ are most advantageous. In the latter case, the Fermi level comes close to the Σ-band edge.

Our calculations give a moderate 30 % gain in absolute value of the Seebeck coefficient in *p*-type material over that in *n*-type at the high temperatures around 800 K.

The full thermal conductivity (Figs. 6, 7) increases with the increase in the carrier concentration, as expected. At low doping levels, when only symmetric L-bands are filled with carriers, the thermal conductivity values of *n*- and *p*-materials do not differ significantly. At higher doping levels, light and fast electrons conduct heat better than heavy and slow holes from the Σ-band but the difference is smaller than one could expect looking just at the mobilities. The reasons are the considerable input from light holes in *p*-type material and effective

Fig. 2. The temperature dependence of the electrical conductivity of *n*-type PbTe for three doping levels, as shown in the *inset*.
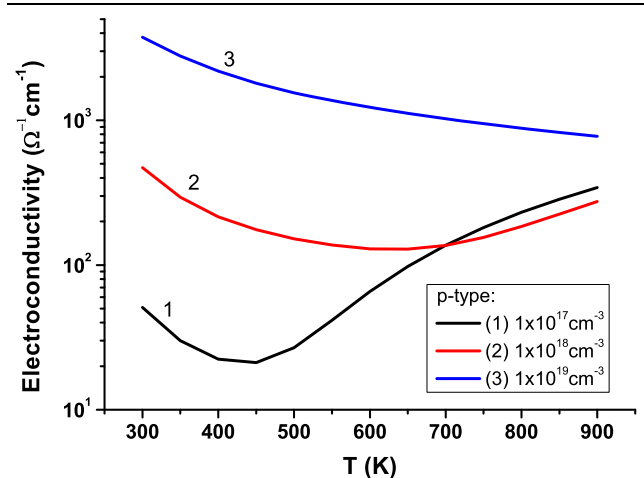

Fig. 3. The temperature dependence of the electrical conductivity of *p*-type PbTe for three doping levels, as shown in the *inset*.
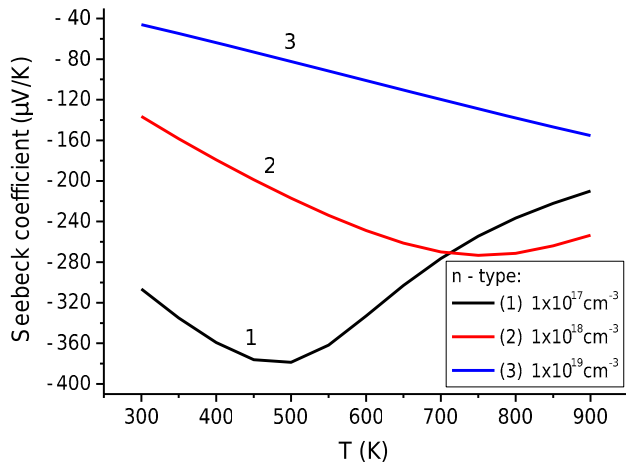
Fig. 4. The temperature dependence of the Seebeck coefficient of *n*-type PbTe for three doping levels, as shown in the *inset*.
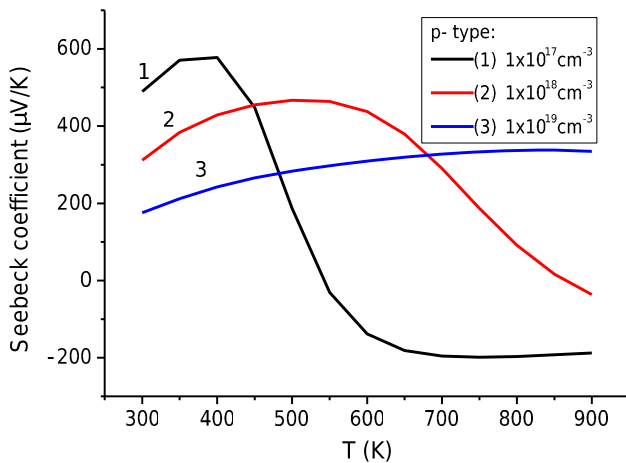

Fig. 5. The temperature dependence of the Seebeck coefficient of *p*-type PbTe for three doping levels, as shown in the *inset*.
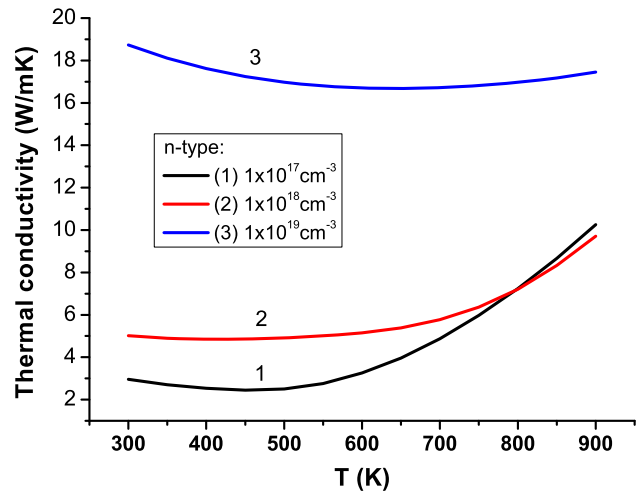

Fig. 6. The temperature dependence of the full thermal conductivity of *n*-type PbTe for three doping levels, as shown in the *inset*.
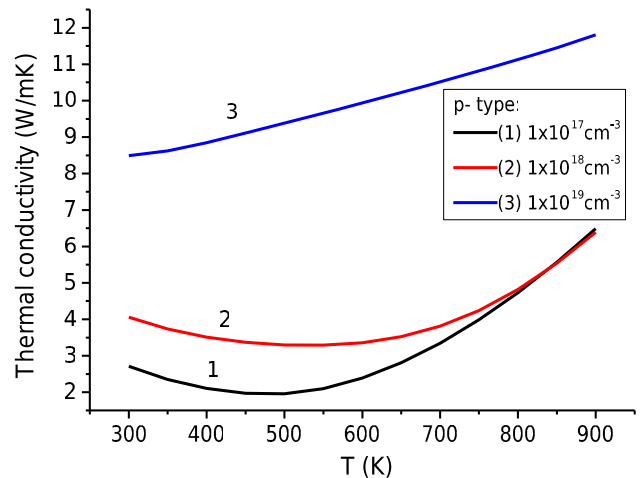

Fig. 7. The temperature dependence of the full thermal conductivity of *p*-type PbTe for three doping levels, as shown in the *inset*.
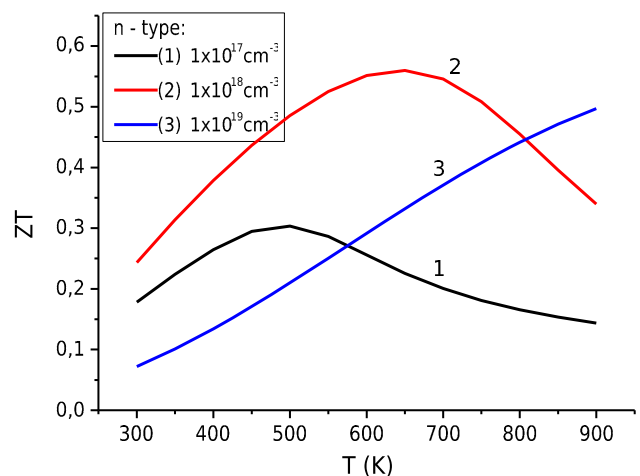

Fig. 8. The temperature dependence of the thermoelectric figure-of-merit of *n*-type PbTe for three doping levels, as shown in the *inset*.

bipolar heat transport mechanism in the three-band spectrum (note the last terms in Eq. 37).

The resulting temperature dependence of the figure-of-merit in *n*- and *p*-type PbTe is shown in Figs. 8 and 9. The positions of ZT maxima correlate with those of the Seebeck coefficient in Figs. 4 and 5. The calculated maximum figure-of-merit value is higher in *p*-type material than in *n*-type one, the difference approaches 30 %. It is not that large because the higher Seebeck coefficient of the heavily doped *p*-type material is partially compensated by the lower heat conductivity of the moderately doped *n*-type material, whereas their electrical conductivities are nearly equal.

We also performed a study of the influence of the particular carrier scattering mechanisms, i.e. of impurity, DA- and PO-scattering, on the thermoelectric properties of PbTe. The most effective scattering channel at elevated temperatures is PO-phonon scattering. If the collision rate of carriers with PO-phonons could be reduced in the
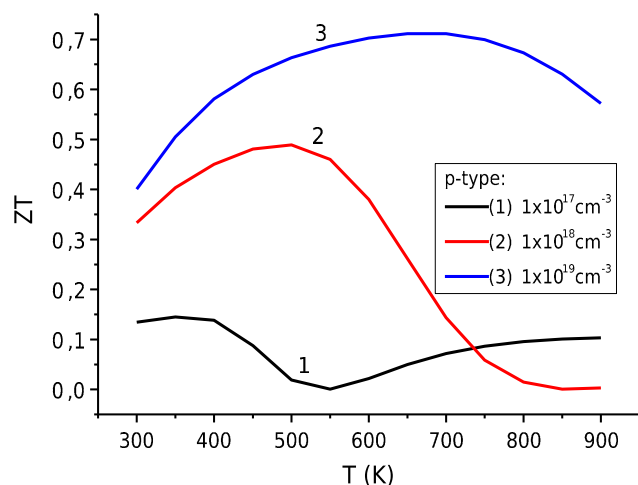
Fig. 9. The temperature dependence of the thermoelectric figure-of-merit of *p*-type PbTe for three doping levels, as shown in the *inset*.

material, its thermoelectric figure-of-merit would increase considerably. These results will be published elsewhere.

One could hardly expect that the simplified isotropic one-valley model of the spectrum used in this work would allow to quantitatively describe experiments carried out on numerous dissimilar samples throughout the entire wide intervals of doping and temperature considered here. But the agreement of our results with the experiment seems generally reasonable for a simple model, being better for some quantities and somewhat worse for others. In general, the model better describes characteristics of *p*-type material than of *n*-type, maybe because the heavy hole Σ-band extrema have smaller anisotropy than the carriers in L-extrema.

The calculated values of the Seebeck coefficient in *p*-type samples are in good agreement with the experimental data presented in Refs. [12] and [15] at 300 K, and are quite close to those measured in heavily acceptor-doped samples,[13] especially at elevated temperatures. Agreement with the experimental data for *n*-type material presented in Refs. [12] and [29] is also not bad.

The calculated electrical conductivity values of *p*-type material are in fair agreement with those measured in heavily doped samples in Ref. [13]. The calculated *n*-type conductivity is, however, higher than typical experimental data, probably due to lack of heavy electron mass in our isotropic model of the spectrum, which leads to a decrease of scattering probability and to a mobility increase. Correspondingly, the calculated heat conductivity is also somewhat higher than the experimental one. But the simultaneous increase of the electrical and heat conductivities does not influence the thermoelectric figure-of-merit (1), and the calculated *ZT* values are in good agreement with typical experimental data for both *n*- and *p*-PbTe.[1,2]

Our calculations did not show a considerable figure-of-merit increase in *p*-type material due to an influence of the heavy hole Σ-band. We were not able to reproduce the high figure-of-merit values obtained in Refs. [13] and [14], the calculated *ZT* value being almost two times lower than was observed there. This may be connected with a non-optimal choice of the Σ-band parameters; they are not known precisely, and their variation would probably somewhat change the results of calculations. It also cannot be ruled out that the high measured *ZT* figures in Refs. [13] and [14] might be caused by a physical mechanism different from the mere Σ-band edge influence.

CONCLUSION

We have calculated the thermoelectric characteristics of PbTe using an isotropic three-band model of its electron energy spectrum. We have taken into account light electrons and holes in L-extrema and heavy holes in Σ-extrema, which allowed us to perform calculations in wide intervals of donor and acceptor doping and of the temperature. The maximum calculated figure-of-merit values were 0.56 for *n*-type material and 0.71 for *p*-type, being very close to typical experimental figures in this material.[1,2]

ACKNOWLEDGEMENT

REFERENCES

1. T.M. Tritt and M.A. Subramanian, *MRS Bull.* 31, 188 (2006).
2. H. Ohita, Mater. *Today* 10, 44 (2007).
3. A.V. Dmitriev and I.P. Zvyagin, *Phys. Uspekhi* 53, 789 (2010).
4. H. Sitter, K. Lishka, and H. Heinrich, *Phys. Rev. B* 16, 680 (1977).
5. E. Skipetrov, E. Zvereva, L. Skipetrova et al., *Phys. Stat. Sol. B* 241, 1100 (2004).
6. E.P. Skipetrov, E.A. Zvereva, B.B. Kovalev et al., *Eur. Phys. J. Appl. Phys.* 29, 23 (2005).
7. E. Skipetrov, A. Golubev, N. Pichugin et al., *Phys. Stat. Sol. B* 244, 448 (2007).
8. P.K. Rawat, B. Paul, and P. Banerji, *Phys. Stat. Sol. RRL* 6, 481 (2012).
9. E.P. Skipetrov, A.N. Golovanov, E.I. Slynko et al., *Low Temp. Phys.* 39, 76 (2013).
10. N.F. Mott and H. Jones, *The Theory of the Properties of Metals and Alloys* (Oxford: Clarendon, 1936).
11. J.P. Heremans, V. Jovovic, E.S. Toberer, A. Saramat, K. Kurosaki, A. Charoenphakdee, S. Yamanaka, and G.J. Snyder, *Science* 321, 554 (2008).
12. A. Ishida, T. Yamada, D. Cao, Y. Inoue, M. Veis, and T. Kita, *J. Appl. Phys.* 106, 023718 (2009).
13. J. Andrulakis, I. Todorov, D.-Y. Chung, S. Ballikaya, G. Wang, C. Uher, and M. Kanatzidis, *Phys. Rev. B* 82, 115209 (2010).
14. Y. Pei, A. LaLonde, S. Iwanga, and G.J. Snyder, *Energy Environ. Sci.* 4, 2085 (2011).
15. A. Ishida, T. Yamada, T. Nakano, Y. Takano, and S. Takaoka, *Jpn. J. Appl. Phys.* 50, 031302 (2011).
16. S.D. Beneslavskii and A.V. Dmitriev, *Solid State Commun.* 32, 1175 (1979).
17. A.I. Anselm, *Introduction to Semiconductor Theory* (Moscow: Mir Publishers & Prentice Hall, 1982).

18. A.V. Dmitriev, *Semicond. Sci. Technol.* 5, 1 (1990).
19. G.D. Mahan and J.O. Sofo, *Proc. Natl. Acad. Sci. USA* 93, 7436 (1996).
20. C.F. Gallo, *J. Appl. Phys.* 36, 3410 (1965).
21. I.A. Smirnov and V.I. Tamarchenko, *Electron Heat Conductivity in Metals and Semiconductors* (Leningrad: Nauka, 1974; in Russian).
22. B.M. Askerov, *Electron Transport Phenomena in Semiconductors* (Singapore: World Scientific, 1994).
23. B.M. Mogilevskii and A.F. Chudnovskii, *Heat Conductivity of Semiconductors* (Moscow: Nauka, 1972; in Russian).
24. R. Dornhaus, G. Nimtz, and B. Schlicht, *Narrow-Gap Semiconductors* (Berlin: Springer, 1983).
25. A. Krotkus and Z. Dobrovolskis, *Electrical Condictivity of Narrow-Gap Semiconductors* (Vilnius: Mokslas, 1988; in Russian).
26. H. Preier, *Appl. Phys.* 20, 189 (1989).
27. B.A. Akimov, A.V. Dmitriev, D.R. Khokhlov, and L.I. Ryabova, *Phys. Stat. Sol. A* 137, 9 (1993).
28. A.V. Dmitriev and A.B. Evlyukhin, *Semicond. Sci. Technol.* 9, 2056 (1994).
29. A. Ishida, D. Cao, S. Morioka, M. Veis, Y. Inoue and T. Kita, *Appl. Phys. Lett.* 92, 182105 (2008).